IEEE TRANSACTIONS ON NANOBIOSCIENCE, VOL. 21, NO. 1, JANUARY 2022

Design and Performance Analysis of Reconfigurable 1D Photonic Crystal Biosensor Employing $Ge_2Sb_2Te_5$ (GST) for Detection of Women Reproductive Hormones

Abinash Panda, D. Vigneswaran, Puspa Devi Pukhrambam, *Member, IEEE*, Natesan Ayyanar, and Truong Khang Nguyen, *Member, IEEE*

***Abstract*—The present research demonstrates a novel 1D photonic crystal (PhC) based reconfigurable biosensor pertaining to label-free detection of different concentrations of progesterone and estradiol, which play a vital role in developing reproductive hormones in women. The proposed sensor is designed by an alternative arrangement of Na_3 AlF_6 and CeO_2, with a central defect layer. A thin layer of novel phase change chalcogenide material (Ge_2 Sb_2 Te_5) is deposited along the two sides of the defect layer to improve the sensing performance. Numerical simulation of transmission spectrum for TE mode is carried out by using the transfer matrix method (TMM). The mainstay of this research is centered on the assay of shift in the defect mode position and intensity with respect to different concentrations of analyte, by changing the phase of the GST material from amorphous to crystalline. Interestingly, we observed a high tunability in defect mode wavelength, when the phase is changed from amorphous to crystalline, which leads to accomplishment of a high sensitivity of 1.75 nm/nmol/L for progesterone and 20.5 nm/nmol/L for estradiol. Aside from sensitivity, other significant parameters like figure of merit and detection limit are computed, which give a deep insight into the sensing performance. These encouraging sensing performances pave the path for efficient detection of different concentrations of progesterone and estradiol to monitor various gynecological problems in women.**

***Index Terms*—Photonic crystal, phase change material, transfer matrix method, defect mode, biosensor.**

I. Introduction

OVER the past two decades, photonic crystal (PhC) structures have come up as a promising candidate to control and manipulate the flow of electromagnetic (EM) waves [1]. The PhCs are artificial structures with periodic arrangement of dielectric layers in space in one dimension (1D), two dimensions (2D) or three dimensions (3D). Compared to the 2D and 3D PhCs, 1D structures have gathered enormous research attention due to their special properties like ease in manufacture, simple structural analysis and cost-effectiveness [2], [3]. Upon interaction with EM signal, 1D PhC exhibits a unique property known as photonic band gap (PBG), which indicates a particular range of wavelength is forbidden to propagate in the structure [4], [5]. Upon insertion of a defect in the layered structure, photons are localized within the PBG, which leads to the formation of resonant mode/defect mode [6]. The width of PBG and position of defect mode are greatly influenced by various structural parameters such as nature of materials, permittivity of materials, thickness of different layers, and angle of incidence of light. The PBG and defect mode characteristics can be manipulated to regulate the transmittance, reflection and absorption spectrum of the 1D PhC structures, which leads to the realization of a wide variety of applications like high performance filters, optical splitters, biosensors, photovoltaic cells, solar cells, optical switches, loss-less photonic waveguides [7]–[10].

Among the aforementioned noteworthy applications, biosensing application is currently in high demand in the research community. Most of the photonic biosensors are analyzed by observing the spectral shift of the resonant mode with respect to the variation in the refractive index (RI) of bio-analytes. The tunability in the position and intensity of the defect mode is basically due to the dependency of RI of the constituted materials and defect layer on the external parameters such as applied voltage, electric field, magnetic field, temperature, and pressure etc. [11]–[13]. A Tamm-Fano resonance-based 1D PhC biosensor is reported by Z.A. Zaky *et al.*, where the authors obtained an ultrahigh sensitivity of 3×10^4 nm/RIU [14]. A. Mehaney *et al.*, investigated the transmittance characteristics of a defected 1D PhC to monitor different concentrations of hydrogen peroxide and glucose in blood [15]. A simple yet effective photonic biosensor is theoretically assayed for early stage detection of tuberculosis diseases with a sensitivity of 1390 nm/RIU [16]. A.H. Aly *et al.* studied a 1D PhC sensor through a

Manuscript received July 15, 2021; revised August 22, 2021; accepted August 22, 2021. Date of publication August 24, 2021; date of current version December 31, 2021. *(Corresponding author: Natesan Ayyanar.)*

Abinash Panda and Puspa Devi Pukhrambam are with the Department of Electronics and Communication Engineering, National Institute of Technology Silchar, Silchar, Assam 788010, India (e-mail: abinashpanda087@gmail.com; puspa.devi@ece.nits.ac.in).

D. Vigneswaran is with the Department of Physics, University College of Engineering, Ramanathapuram Campus, Pullangudi, Tamil Nadu 623513, India (e-mail: dhasa.viki@gmail.com).

Natesan Ayyanar and Truong Khang Nguyen are with the Division of Computational Physics, Institute for Computational Science, Ton Duc Thang University, Ho Chi Minh City 756636, Vietnam, and also with the Faculty of Electrical and Electronics Engineering, Ton Duc Thang University, Ho Chi Minh City 756636, Vietnam (e-mail: ayyanar@tdtu.edu.vn; nguyentruongkhang@tdtu.edu.vn).

Digital Object Identifier 10.1109/TNB.2021.3107592

detailed analysis of transmission characteristics, where the authors analyzed the transmission spectra of 1D PhC by using TMM approach to detect various concentrations of creatinine in blood [12]. A hybrid defective one-dimensional PhC is reported by A.H. Aly and his team for sensing different concentrations of sugar present in blood [10]. The authors employed TMM for optimization of various structural parameters and attained a maximum sensitivity of 1100 nm/RIU. A new metal-based 1D PhC configuration is demonstrated for realization of gas sensing application [17]. In this reference, the authors explored the significance of metal layer for the generation of plasmon resonance within the photonic band gap, and they obtained a high sensitivity of $1.9 \times 10^5 \frac{nm}{RIU}$ and low a detection limit of $1.4 \times 10^{-7} RIU$. In the last few years, 1D PhC structures are widely researched for effective detection of various biological molecules, blood cells, enzymes, bacteria, drugs, different cancer cells [18]–[23]. Therefore, 1D PhC based biosensors are going to rule the future biomedical industries.

Over the years, researchers have successfully designed and tested PhC based biosensors with a variety of materials like semiconductors, polymers, metamaterials, superconductors, plasmas, graphene, TMDC group materials [24]–[26]. However, these sensors are underperformed in case of multiple biomolecules detection. On the other hand, relatively new class of sensors like reconfigurable sensors [28] and multimode sensors [27] are the best options for detection of multiple biomolecules, where the sensitivity can be adjusted from minimum to maximum. Moreover, different biosensing applications have been reported earlier by employing GST-based reconfigurable phase change material [49]–[51].

Inspired by the above-mentioned notable works, in this article, we are encouraged to design and analyse phase change material (PCM) based reconfigurable 1D PhC sensor for monitoring of the progesterone and estradiol concentrations in women. The nanophotonic platform integrated with PCM has numerous merits compared to other functional materials, owing to its reliable and repeatable switching ability through electrically or optically [29]–[31]. $Ge_2Sb_2Te_5$ (GST) is one of such PCM, which is highly scalable, stable, non-volatile, and smoothly integrated with other optoelectronic devices. The most attractive property of GST is that its optical functionalities can be significantly altered by switching the phase from amorphous to crystalline [32], [33]. Additionally, both of these phases are stable at ambient temperature and can be reversibly switched at sub nanosecond time scale. Apart from this, GST exhibits good stability in any intermediate state between amorphous and crystalline phase by effectively governing the time of external stimulus, which leads to realization of metasurfaces based tunable nanophotonic devices [34]. By precisely manipulating the intermediate phase of GST, the multimodal nature of GST can be explored to envisage various applications such as photonic switches, sensors, modulators etc [35]. These attractive features of GST offers a high degree of freedom with improved performance compared to the mechanically adjusted optical devices and liquid crystals.

In this article, for the first time, we propose a novel GST based reconfigurable 1D PhC sensor for identification of reproductive hormones in the women blood samples. This research has couple of newness compared to earlier published works. A detailed performance analysis is carried out by considering GST material along the two sides of the defect layer, which is the prime novelty of the present work. Besides this, the most important women reproductive hormones like progesterone and estradiol are taken as bioanalytes, which further enhances the novelty of this work. As GST shows a high refractive index contrast between its amorphous and crystalline phases, so this material can be a good candidate to envisage tunable biosensor. A detailed assay of transmission characteristics is performed by changing different geometrical parameters like thickness of defect layer and incident angle. The mainstay of the present research is to assay the shift in the position (wavelength) of the defect mode with respect to different progesterone and estradiol concentrations. Moreover, the proposed sensor shows superior defect mode wavelength tunability by altering the phase of GST from amorphous to crystalline, which leads to high sensing performances compared to the previously published research works.

II. Sensor Design and Numerical Analysis

The schematic diagram of the proposed 1D PhC sensor is represented in figure 1. It is essential to highlight that the sensor is designed with two binary PhCs such as PhC1 and PhC2, consisting of an alternate arrangements of identical materials of Na_3AlF_6 (cryolite) and CeO_2 (cerium oxide). A defect layer (air medium), whose two sides are coated with phase change chalcogenide material of GST, is sandwiched between the PhC1 and PhC2 such that the sensor configuration is in the form $(AB)^N GDG(AB)^N$. The letters A, B, G, D indicate Na_3AlF_6, CeO_2, GST and defect layer respectively. The alphabet N signifies the period, which is taken as N = 5 in the present work. The entire structure is placed between the air medium. The thickness of different layers are carefully optimized in order to achieve maximum band gap and high sensing performances. We have considered the thickness of Na_3AlF_6, CeO_2, GST and defect layer as $d_A = 355\ nm$, $d_B = 270\ nm$, $d_G = 78\ nm$ and $d_D = 420\ nm$ respectively. The refractive index of Na_3AlF_6 and CeO_2 are considered as $n_A = 1.34$ and $n_B = 2.4$. Blood sample is infiltrated in the central defect layer for measuring hormones. We have considered that a plane wave strikes on the suggested structure at an angle of θ_{in} with reference to z-axis.

We assayed the sensing performances for both crystalline and amorphous phases of the GST material, where the refractive indices were experimentally evaluated using spectroscopic ellipsometry (J. A. Woollam Co., Inc, V-VASE). The experimentally calculated and fitted RI value of GST is shown in Fig. 2 (a).

For an experimental investigation of GST index values for both the phases, 20 nm GST thin film is coated on the silicon substrate and its n, k values are extracted from ellipsometry followed Tauc-Lorentz model. Since we need to demonstrate the tunability, the phase of GST should be switched from

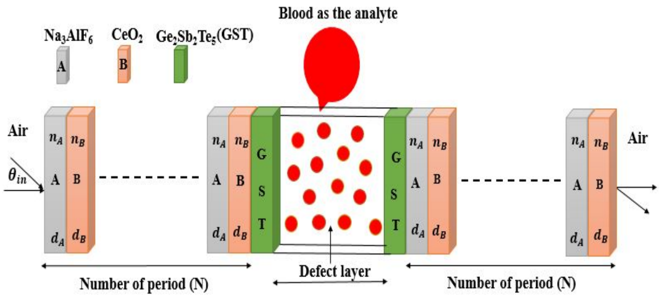

Fig. 1. The schematic design of the 1D PhC sensor with configuration $(AB)^N GDG(AB)^N$.

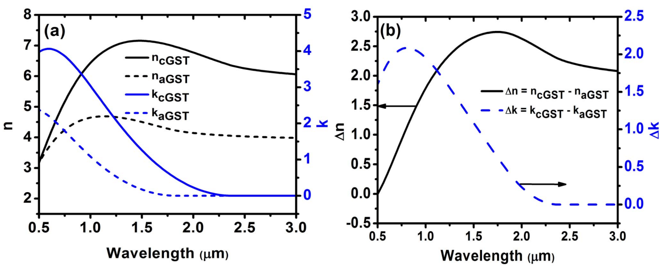

Fig. 2. Experimentally calculated (a) Complex refractive indices of aGST and cGST (b) Refractive index difference between aGST and cGST.

amorphous phase to crystalline phase, which is possible by different methods such as heating the sample at 160°C for 60 min, laser induced heating at nanosecond time scales, optical pumping, electric current [36], [37]. This phase change can be achieved in a very small time duration (less than 30 ns) with high stability. Here, the authors want to assure that phase change is possible by applying thermal stimuli only across the GST material for a very small time span of less than 30 ns, which will not affect the optical properties of other dielectric materials and analytes in the structure. The crystalline GST was fitted using a Tauc-Lorentz oscillator model. There is a significant variation in both n and k values by switching from amorphous phase (aGST) to crystalline phase (cGST). Fig. 2 (b) shows the refractive index difference between aGST and cGST. From this figure, we have noted maximum changes in complex refractive index (Δn & Δk) in the near-infrared (NIR) wavelengths, therefore it can be used as a tunable optical material in the photonic crystal sensor to tune the refractive index sensitivity.

In the proposed PhC biosensor, the blood samples to be sensed are considered for women's reproductive hormones namely progesterone and estradiol. Progesterone is a steroid hormone that is highly significant in the detection and maintenance of pregnancy in women. They perform a dominant role in the reproductive process of females as ovulation and pregnancy [38]. This hormone develops the uterus for embedding of fertilized ovum and allows the mammary glands glandular elements to grow in secretory epithelium with effect of action along with other hormones as prolactin to assist in production of milk [39]. Further, at late pregnancy, progesterone is entirely yielded by the placenta, which is highly responsible for the development of fetus [40]. Estradiol also plays a prominent role in pregnancy [41]. It is the most abundant and strongest

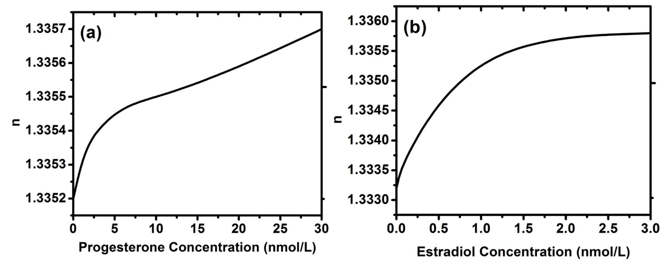

Fig. 3. Experimentally calculated RI values for different (a) progesterone and (b) estradiol hormones concentration level.

form of estradiol which provokes maturation and release of the egg from the ovary which is generated by the corpus luteum. The estradiol assists and supports in thickening the lining of the uterus which permits the fertilized egg to get embedded [42], [43].

Experimentally determined RI of progesterone and estradiol hormone concentration level is used in the theoretical analysis. The RI of progesterone and estradiol hormone concentration level in blood sample is measured by pocket refractometer (Atago PAL-RI) as shown in Fig.3.

TMM is the best suited technique to describe the characteristics of the EM waves while propagating between different layers of the proposed multilayer structure. In this technique, each layer is represented in matrix form, which is a function of layer refractive index and thickness. The overall transfer matrix is computed by multiplying the individual matrix of each layer. For the layers A, B, G and D, the transfer matrix can be written as [44],

$$M_k = \begin{bmatrix} cos\rho_k & \left(-\frac{i}{\varphi_k}\right) sin\rho_k \\ -i\varphi_k sin\rho_k & cos\rho_k \end{bmatrix} \quad (1)$$

where, k denotes various layers A, B, G and D. ρ_k is defined as [44],

$$\rho_k = \frac{2\pi}{\lambda} d_k n_k cos\theta_k \quad (2)$$

Here, d_k, n_k and θ_k signify the thickness, refractive index and angle of incidence of the k^{th} layer respectively. Further, λ denotes the free space wavelength. In equation (1), φ_k is defined as $\varphi_k = z_0 n_k cos\theta_k$ for TE mode and $\varphi_k = \frac{cos\theta_k}{z_0 n_k}$ for TM mode, where z_0 signifies the free space impedance. The transfer matrix of the complete structure is defined as [45],

$$M = \begin{bmatrix} M_{11} & M_{12} \\ M_{21} & M_{22} \end{bmatrix} = (M_A M_B)^N M_G M_D M_G (M_A M_B)^N \quad (3)$$

Here, M_A, M_B, M_G and M_D symbolize the respective transfer matrix of Na_3AlF_6, CeO_2, $Ge_2Sb_2Te_5$ and defect layer. From equation (3), the transmittance coefficient can be specified as [46],

$$t = \frac{2\gamma_0}{\left(M_{11} + M_{12}\gamma_y\right)\gamma_0 + \left(M_{21} + M_{22}\gamma_y\right)} \quad (4)$$

where, γ_0 and γ_y signify the incidenting and transmitting medium of the proposed structure. In case of TE wave, γ_0 and γ_y can be defined as, $\gamma_0 = z_0 n_0 cos\theta_{in}$ and $\gamma_y = z_0 n_y cos\theta_y$.

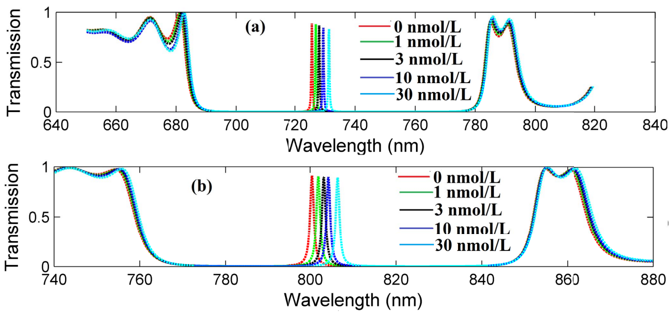

Fig. 4. Transmission spectrum of the proposed sensor for different progesterone concentration (a) aGST (b) cGST phase at $d_D = 420$ nm.

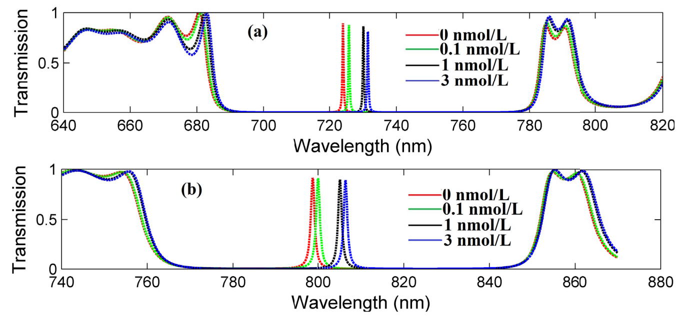

Fig. 5. Transmission spectrum of the proposed sensor for different estradiol concentration (a) aGST (b) cGST phase at $d_D = 420$ nm.

Finally, transmittance (T) of the entire structure can be computes as [46],

$$T = \frac{\psi_y}{\psi_0}\left|t^2\right| \tag{5}$$

The effectiveness of the sensor can be perfectly judged by computing different performance measuring parameters like figure of merit (FOM), sensitivity, and detection limit (DL). Sensitivity can be computed by dividing the change in defect mode wavelength by the corresponding change in the refractive index of bio-analyte, which can be stated as [47],

$$S\left(nm/RIU\right) = \frac{\Delta\lambda_{res}}{\Delta n} \tag{6}$$

FOM is defined as the ability to detect the minimum change in the defect mode resonance wavelength, which can be expressed as [48],

$$FOM = \frac{S}{\Delta\lambda_{1/2}} \tag{7}$$

where, $\Delta\lambda_{1/2}$ signifies the spectral half-width of the transmission dip. DL is the sensor ability to detect very small refractive index contrast of the analyte, which is given as [48],

$$DL = \frac{R}{S} \tag{8}$$

where, R is the resolution of the sensor.

III. Results and Analysis

By considering the geometrical parameters as described in section 2, we examined the transmittance characteristics of the suggested 1D PhC by using TMM. Additionally, the effects of variation in thickness of the defect layer and incident angle on the transmittance spectrum are thoroughly examined for both aGST and cGST phase conditions.

Fig. 4 and fig. 5 depict the transmittance spectrum of the suggested 1D PhC sensor by infiltrating the defect medium with different concentrations of progesterone and estradiol hormones respectively. The characteristics of the resonant mode is thoroughly investigated for both aGST and cGST phase. Here, an interesting variation in the position (wavelength) of the defect mode is noticed in case of two phase conditions. The defect modes are observed in the visible wavelength range for aGST and when the phase is switched to cGST, the defect modes are perceived at NIR wavelength range. The aforementioned findings are supported only at the optimized values of structure parameters. Further, it is declared that wavelength of the defect mode is red-shifted for higher concentrations of progesterone and estradiol hormones. Also, it is seen that intensity of defect mode is decreased as we increase the analyte concentration in the defect layer. As we perceived a significant tunability in wavelength and intensity of the resonant mode, by changing the phase of the GST material from amorphous phase to crystalline phase, the proposed sensor can be a suitable choice for refractive index based sensing applications.

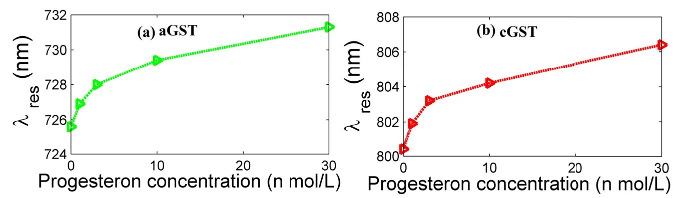

Fig. 6. Variation in wavelength of the resonant mode with respect to different progesterone concentrations.

The primary reason behind the shift in the wavelength of the defect mode is the modification in the effective refractive index of the defect layer with respect to different concentrations of progesterone and estradiol, which changes the transfer matrix of the entire structure. Also, this variation can be well understood by the standing wave condition [45], which is stated as $\Delta = m\lambda = n_{eff}G$, where, Δ and G are the optical path difference and geometrical path difference respectively. n_{eff} is the effective refractive index and m is an integer.

Fig. 6 and fig. 7 display the variation in resonance wavelength (λ_{res}) of the defect mode as we infiltrated the defect layer with different concentrations of progesterone and estradiol respectively. In particular, for aGST, we perceived that defect mode resonance wavelength shifts from 725.6nm to 726.9nm to 728.1nm to 729.4nm to 731.3nm for change in the concentration of progesterone from 0nmol/L to 1nmol/L to3nmol/L to 10nmol/L to 30nmol/L. Similarly, for cGST, we noticed that defect mode resonance wavelength shifts from 800.4nm to 801.9nm to 803.2nm to 804.2nm to 806.4nm for change in the concentration of progesterone from 0nmol/L to 1nmol/L to 3nmol/L to 10nmol/L to 30nmol/L. So, by switching the phase from aGST to cGST, we obtained a notable resonance wavelength tunability i.e. 74.8 nm and 75.1 nm at 0nmol/L and 30nmol/L respectively. The aforementioned

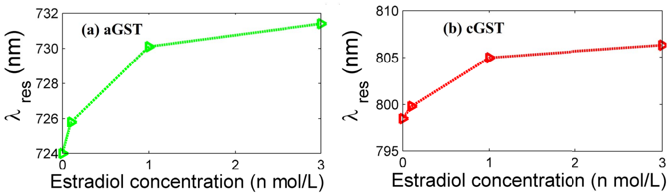

Fig. 7. Variation in wavelength of the resonant mode with respect to different estradiol concentrations.

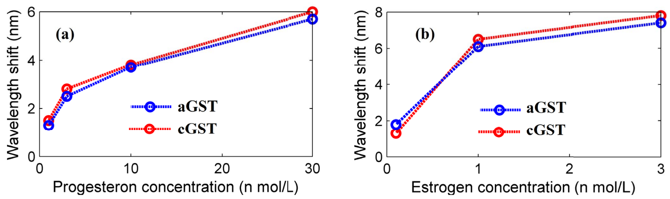

Fig. 8. Defect mode wavelength shift with respect to different progesterone and estradiol concentrations.

variations in defect mode wavelength (λ_{defect}) with respect to the concentration of progesterone is found to be linearly fitted with the following equations:

$$\lambda_{defect} = 0.1627 \times C + 726.81 : \text{aGST}$$
$$\lambda_{defect} = 0.1667 \times C + 801.75 : \text{cGST}$$

Similarly, in case of infiltration with estradiol concentrations (fig. 7), for the aGST phase, the defect mode wavelength shifts from 724.0nm to 725.8nm to 730.1nm to 731.4nm for change in the estradiol concentration from 0nmol/L to 0.1nmol/L to 1nmol/L to 3nmol/L. Similarly, for the case of cGST, we observed that the defect mode wavelength shifts from 798.5nm to 799.8nm to 805.0nm to 806.3nm for change in the estradiol concentration from 0nmol/L to 0.1nmol/L to 1nmol/L to 3nmol/L. The obtained wavelength tunability from aGST to cGST is 74.5 nm and 74.9 nm for 0.1 nmol/L and 3 nmol/L respectively. The aforesaid linear shift in defect mode wavelength (λ_{defect}) is fitted with the following equations:

$$\lambda_{defect} = 2.203 \times C + 725.57 : \text{aGST}$$
$$\lambda_{defect} = 2.4176 \times C + 799.92 : \text{cGST}$$

After the computation of the wavelength associated with defect mode (fig. 6 and fig. 7), we evaluated the shift in the defect mode wavelength for different concentrations of progesterone and estradiol, with reference to the 0 nmol/L, for both phases of the GST layer, which is shown in fig. 8. From this figure, it is declared that for both aGST and cGST wavelength shift increases with increase in analyte concentrations. For progesterone hormone, we noticed a highest wavelength shift of 5.7 nm and 6.0 nm for aGST and cGST respectively, whereas for estradiol hormone, we observed a highest wavelength shift of 7.4 nm and 7.8 nm for aGST and cGST respectively.

Next, we studied the change in the position of the defect mode by varying the defect layer thickness. Figure 9 and figure 10 demonstrate the shifting nature of the defect mode wavelength with respect to different thickness of the defect

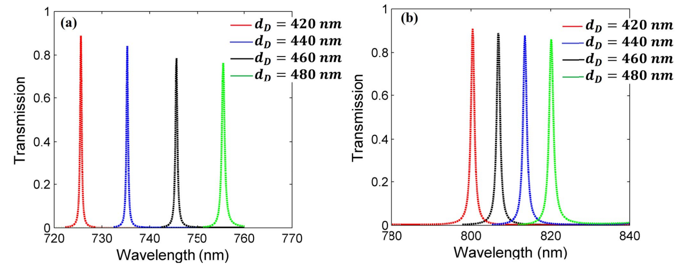

Fig. 9. Shift in defect mode position w.r.t. defect layer thickness for progesterone solution (a) aGST (b) cGST.

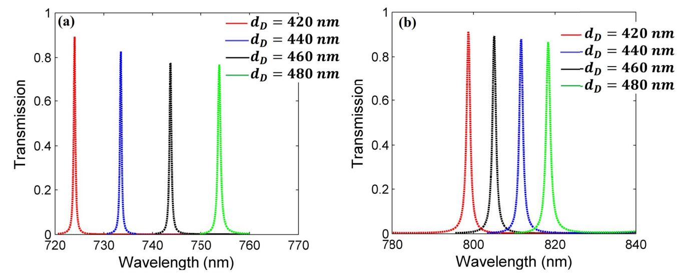

Fig. 10. Shift in defect mode position w.r.t. defect layer thickness for estradiol solution (a) aGST (b) cGST.

layer (d_D) in case of infiltration of blood sample with progesterone and estradiol hormones respectively. We studied the transmittance spectrum under four different thickness values of the defect layer i.e. 420nm, 440nm, 460nm and 480nm. The reason for selecting these thickness values is that perfect defect mode characteristics are obtained only at these values of d_D. It is seen that wavelength of the defect mode is red-shifted with increase in d_D. The reason behind such nature of shifting is increment in the geometrical path difference with increase in d_D. Also, this type of shifting behaviour is experimentally verified by Chu *et al.* [37]. Besides this, it can be noticed that power of the defect mode with rise in d_D.

We investigated the absorption spectrum of the sensor at $d_D = 420\ nm$ and $\theta_{in} = 0^o$, for both aGST and cGST phase, which is represented in fig. 11. From the absorption spectrum it is noticed that the defect mode is formed exactly at the same wavelength as that of the transmission spectrum (fig. 4 and 5). However, the absorption intensity, which is marked within the figure, is very less. Most importantly, it is observed that the absorption intensity increases from 0.0277 to 0.0381 for progesterone hormone and 0.0266 to 0.0372 for estradiol hormone, by switching the phase from aGST to cGST. From the aforementioned findings, we concluded that the proposed sensor in cGST phase suffers higher absorption loss compared to aGST phase.

Fig. 12: Sensitivity of the proposed sensor in (a) aGST and (b) cGST for progesterone concentrations at $\theta_{in} = 0^o$ Fig. 12 and fig. 13 delineate the variation in sensitivity (nm/nmol/L) of the proposed sensor with respect to different thickness of the defect layer (d_D), when the defect layer is infiltrated with progesterone and estradiol hormones respectively. It is worth noticing that sensitivity increases with increase in d_D. This rise in the sensitivity is due to the increment in

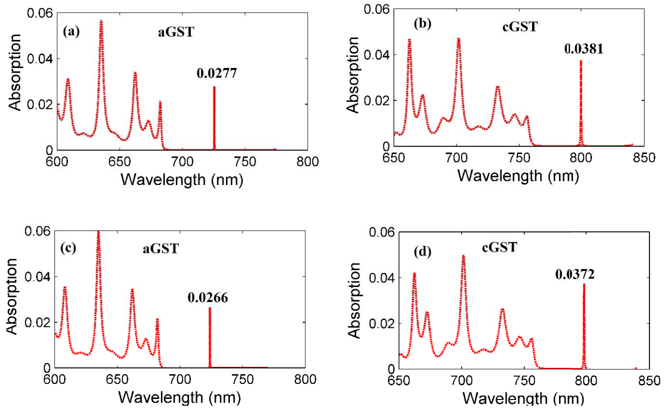

Fig. 11. Absorption spectrum of the proposed sensor at $d_D = 420nm$ and $\theta_{in} = 0°$ (a)-(b) progesterone hormone (c)-(d) estradiol hormone.

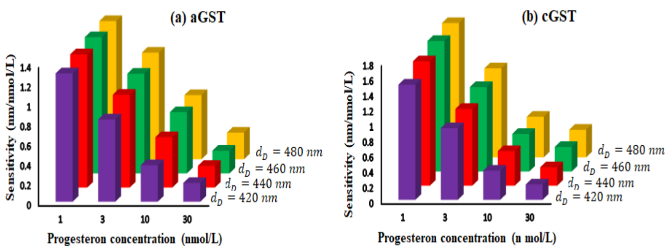

Fig. 12. Sensitivity of the proposed sensor in (a) aGST and (b) cGST for progesterone concentrations at $\theta_{in} = 0°$.

geometrical path difference as d_D increases. For the case of progesterone analyte, maximum sensitivity of 1.4 nm/nmol/L and 1.75 nm/nmol/L are obtained for amorphous phase and crystalline phase of the GST material respectively at $d_D = 480\ nm$. On the other hand, the case of estradiol analyte, optimum sensitivity of 18.4 nm/nmol/L and 20.5 nm/nmol/L are obtained at $d_D = 480\ nm$ for amorphous phase and crystalline phase of the GST material respectively. Therefore, it is clearly understood that there is a considerable enhancement in sensitivity by switching the phase from amorphous to crystalline. In specific, we have obtained better tunability with one time maximize in sensitivity by switching from aGST to cGST. Apart from this, we numerically calculated the sensitivity in terms of nm/RIU, by computing the shift in defect mode wavelength with respect to the change in refractive index of different analyte concentrations. We found that for progesterone hormone, maximum refractive index sensitivity increases from 14000 nm/RIU to 16000 nm/RIU as we switch the phase from aGST to cGST, whereas for estradiol hormone maximum refractive index sensitivity increases from 3333.3 nm/RIU to 3799.1 nm/RIU as we switch the phase from aGST to cGST.

Afterwards, we investigated the effect of change in incident angle on the transmittance characteristics. Fig. 14 and fig. 15 show the colormap plot of transmittance spectrum with respect to incident angle and wavelength for different concentrations of progesterone and estradiol respectively. It can clearly noticed that with an increase in the angle of incidence, the wavelength associated with the defect mode shifts towards lower wavelength. Specifically, in case of amorphous phase,

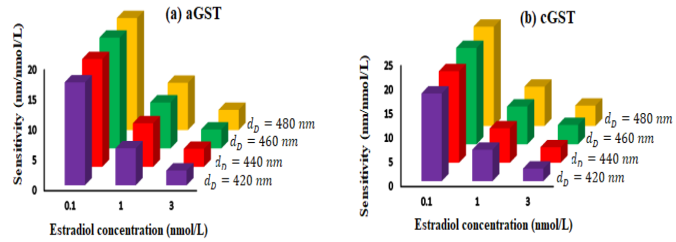

Fig. 13. Sensitivity of the proposed sensor in (a) aGST and (b) cGST for estradiol concentrations at $\theta_{in} = 0°$.

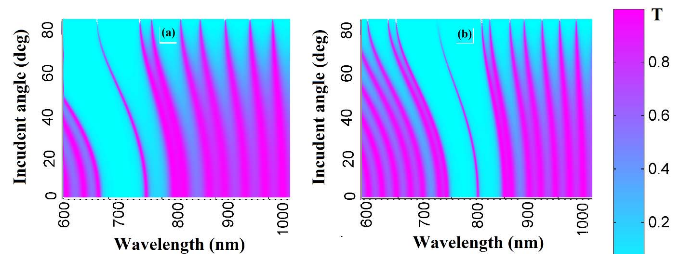

Fig. 14. Colormap plot of transmittance with respect to wavelength and incident angle for 30 nmol/L concentrations of progesterone at $d_D = 480nm$ (a) aGST (b) cGST.

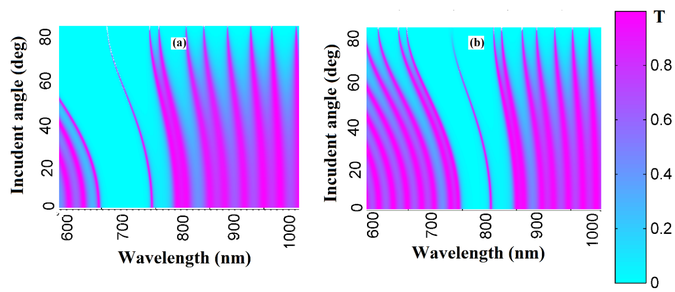

Fig. 15. Colormap plot of transmittance with respect to wavelength and incident angle for 3 nmol/L concentrations of estradiol at $d_D = 480$nm (a) aGST (b) cGST.

there is relatively more shift in defect mode wavelength as compared to the crystalline phase. The above mentioned nature of variation can be well explained by the Bragg Snell's law [46], which is given as, $m\lambda = 2d\sqrt{n_{eff}^2 - sin^2\theta}$, where m, d and θ denote the constructive diffraction order, period of the proposed structure and incident angle respectively.

Eventually, we evaluated the performance measuring parameters of the senor like FOM and DL at $d_D = 480\ nm$ for both progesterone and estradiol concentrations which are state in table I and table II respectively. The proposed progesterone sensor and estradiol sensor delivers FOM in the order of 10^4 and 10^3 respectively, whereas the respective sensors bestows DL in the order of 10^{-5} and 10^{-4} respectively. Nevertheless, sensitivity is higher for crystalline phase (fig. 12 and 13), but FOM and DL is higher for amorphous phase. The primary reason behind this is the inverse dependency of FOM and DL on the $\Delta\lambda_{1/2}$ (Eq. 7-8). As we observed a higher $\Delta\lambda_{1/2}$ for crystalline phase (fig. 4 and 5), so FOM and DL are lower in this case.

TABLE I
FOM AND DL FOR PROGESTERONE SENSOR AT $d_D = 480$NM

Progesterone concentration (nmol/L)	Amorphous phase		Crystalline phase	
	FOM (1/RIU) x10^4	DL (RIU) x10^{-5}	FOM (1/RIU) x10^4	DL (RIU) x 10^{-5}
1	3.500	1.37	1.333	4.84
3	3.178	1.18	1.115	4.88
10	2.660	1.36	0.976	5.18
30	2.496	1.30	0.896	5.10

TABLE II
FOM AND DL FOR ESTRADIOL SENSOR AT $d_D = 480nm$

Estradiol concentration (nmol/L)	Amorphous phase		Crystalline phase	
	FOM (1/RIU) x10^3	DL (RIU) x10^{-4}	FOM (1/RIU) x10^3	DL (RIU) x 10^{-4}
0.1	7.59	4.12	2.15	6.22
1	6.18	4.47	2.22	6.04
3	6.13	4.66	2.29	5.91

TABLE III
COMPARATIVE ANALYSIS OF OPTIMUM SENSOR PERFORMANCES

Sensing analyte	Sensitivity (nm/RIU)	FOM (1/RIU)	DL (RIU)	Refer ence
Waterborne bacteria	387.5	1174.24	2.44×10^{-4}	[7]
Alcohol sensor	873	290	---------	[19]
Soybean biodiesel	277.7	1322	0.10×10^{-3}	[21]
Biomedical fluids	6770	398	4.5×10^{-3}	[22]
Hemoglobin sensor	167	0.63	---------	[48]
Sucrose	1016.35	----------	2.28×10^{-4}	[47]
Women reproductive hormones	16000	1.33 $\times 10^4$	4.84×10^{-5}	This work

Finally, the major performance of the proposed 1D sensor is compared with recently published similar types of works and the comparative analysis is represented in table III. As, stated in this table, the proposed senor delivers maximum sensitivity, FOM and DL, which proves the significance of this work in the research domain of biosensors and biophotonics.

IV. CONCLUSION

We theoretically examined the transmittance spectrum of the proposed multilayer structure having configuration $(Na_3AlF_6/CeO_2)^N/Ge_2Sb_2Te_5/Defect/Ge_2Sb_2Te_5/(Na_3AlF_6/CeO_2)^N$ for sensing the bio-analytes like progesterone and estradiol. Geometrical parameters like thickness of dielectric layers, thickness of defect layer, incident angle, and number of period are properly optimized to attain high sensing performances. We investigated the sensing characteristics by switching the phase of the GST material from crystalline to amorphous phase. At the optimized structure parameters, we perceived that, within the PBG, the defect modes are formed in the visible wavelength range for amorphous phase, whereas, the defect modes are perceived at NIR wavelength range for the crystalline phase. This significant wavelength tunability between aGST and cGST, leads to high sensitivity, FOM and DL. Further, we noticed that optimum sensing performance is obtained at normal incidence of the EM wave with a defect layer thickness of 480 nm. Specifically, for the case of progesterone analyte, maximum sensitivity increases from 1.4 nm/nmol/L to 1.75 nm/nmol/L, and for estradiol analyte, the optimum sensitivity increases from 18.4 nm/nmol/L to 20.5 nm/nmol/L, by switching the phase from aGST to cGST. A comparative analysis of sensor performance is carried out to prove the superiority of the proposed sensor. Lastly, by realising the importance of accurate detection of progesterone and estradiol hormones in women, the simple structure, easy analysis and available fabrication techniques make the proposed sensor worth fabricating.

REFERENCES

[1] E. Yablanovitch, "Inhibited spontaneous emission in solid state physics and electronics," *Phys. Rev. Lett*, vol. 58, pp. 2059–2062, 1987.
[2] F. S. Chaves and H. V. Posada, "Transmittance spectrum of a superconductor-semiconductor quasiperiodic one-dimensional photonic crystal," *Phys. C, Supercond. Appl.*, vol. 18, p. 30462, Aug. 2019.
[3] O. A. Abd El-Aziz, H. A. Elsayed, and M. I. Sayed, "One-dimensional defective photonic crystals for the sensing and detection of protein," *Appl. Opt.*, vol. 58, no. 30, pp. 8309–8315, 2019.
[4] S. Li, H. Lin, F. Meng, D. Moss, X. Huang, and B. Jia, "On-demand design of tunable complete photonic band gaps based on bloch mode analysis," *Sci. Rep.*, vol. 8, no. 1, p. 14283, Dec. 2018.
[5] M. N. Armenise, C. E. Campanella, C. Ciminelli, F. Dell'Olio, and V. M. N. Passaro, "Phononic and photonic band gap structures: Modelling and applications," *Phys. Procedia*, vol. 3, no. 1, pp. 357–364, Jan. 2010.
[6] A. H. Aly, F. A. Sayed, and H. Elsayed, "Defect mode tunability based on the electro-optical characteristics of the one-dimensional graphene photonic crystals," *Appl. Opt.*, vol. 59, no. 16, pp. 4796–4805, Jun. 2020.
[7] A. Panda and P. D. Pukhrambam, "Investigation of defect based 1D photonic crystal structure for real-time detection of waterborne bacteria," *Phys. B, Condens. Matter*, vol. 607, no. 3, Apr. 2021, Art. no. 412854.
[8] A. Panda, P. Sarkar, and G. Palai, "Research on SAD-PRD losses in semiconductor waveguide for application in photonic integrated circuits," *Optik*, vol. 154, pp. 748–754, Feb. 2018.
[9] F. Ghasemi, S. R. Entezar, and S. Razi, "Terahertz tunable photonic crystal optical filter containing graphene and nonlinear electro-optic polymer," *Laser Phys.*, vol. 29, no. 5, May 2019, Art. no. 056201.
[10] A. H. Aly, Z. A. Zaky, A. S. Shalaby, A. M. Ahmed, and D. Vigneswaran, "Theoretical study of hybrid multifunctional one-dimensional photonic crystal as a flexible blood sugar sensor," *Phys. Scripta*, vol. 95, no. 3, Mar. 2020, Art. no. 035510.
[11] Z. A. Zaky and A. H. Aly, "Theoretical study of a tunable low-temperature photonic crystal sensor using dielectric-superconductor nanocomposite layers," *J. Supercond. Novel Magn.*, vol. 33, no. 10, pp. 2983–2990, Oct. 2020.
[12] A. H. Aly, D. Mohamed, M. A. Mohaseb, N. S. A. El-Gawaad, and Y. Trabelsi, "Biophotonic sensor for the detection of creatinine concentration in blood serum based on 1D photonic crystal," *RSC Adv.*, vol. 10, no. 53, pp. 31765–31772, 2020.

[13] C. Zeng, C. Luo, L. Hao, and Y. Xie, "The research on magnetic tunable characteristics of photonic crystal defect localized modes with a defect layer of nanoparticle magnetic fluids," *Chin. Opt. Lett.*, vol. 12, Jul. 2014, Art. no. S11602.

[14] Z. A. Zaky, A. Sharma, S. Alamri, and A. H. Aly, "Theoretical evaluation of the refractive index sensing capability using the coupling of Tamm–Fano resonance in one-dimensional photonic crystals," *Appl. Nanosci.*, vol. 11, no. 8, pp. 2261–2270, Jul. 2021.

[15] A. Mehaney, A. Nagaty, and A. H. Aly, "Glucose and hydrogen peroxide concentration measurement using 1D defective phononic crystal sensor," *Plasmonics*, Apr. 2021, doi: 10.1007/s11468-021-01435-4.

[16] A. H. Aly *et al.*, "Novel biosensor detection of tuberculosis based on photonic band gap materials," *Mater. Res.*, vol. 24, no. 3, 2021, Art. no. e20200483.

[17] Z. A. Zaky, A. M. Ahmed, A. S. Shalaby, and A. H. Aly, "Refractive index gas sensor based on the Tamm state in a one-dimensional photonic crystal: Theoretical optimisation," *Sci. Rep.*, vol. 10, no. 1, p. 9736, Dec. 2020.

[18] W. M. Nouman, S. E.-S. Abd El-Ghany, S. M. Sallam, A.-F.-B. Dawood, and A. H. Aly, "Biophotonic sensor for rapid detection of brain lesions using 1D photonic crystal," *Opt. Quantum Electron.*, vol. 52, no. 6, p. 287, Jun. 2020.

[19] S. M. Shaban, A. Mehaney, and A. H. Aly, "Determination of 1-propanol, ethanol, and methanol concentrations in water based on a one-dimensional phoxonic crystal sensor," *Appl. Opt.*, vol. 59, no. 13, pp. 3878–3885, 2020.

[20] A. H. Aly and Z. A. Zaky, "Ultra-sensitive photonic crystal cancer cells sensor with a high-quality factor," *Cryogenics*, vol. 104, Dec. 2019, Art. no. 102991.

[21] H. A. Elsayed and A. Mehaney, "Monitoring of soybean biodiesel based on the one-dimensional photonic crystals comprising porous silicon," *Appl. Nanosci.*, vol. 11, no. 1, pp. 149–157, Jan. 2021.

[22] A. Mehaney, M. M. Abadla, and H. A. Elsayed, "1D porous silicon photonic crystals comprising Tamm/Fano resonance as high performing optical sensors," *J. Mol. Liquids*, vol. 322, Jan. 2021, Art. no. 114978.

[23] B.-F. Wan, Z.-W. Zhou, Y. Xu, and H.-F. Zhang, "A theoretical proposal for a refractive index and angle sensor based on one-dimensional photonic crystals," *IEEE Sensors J.*, vol. 21, no. 1, pp. 331–338, Jan. 2021.

[24] A. H. Aly, A. Aghajamali, H. A. Elsayed, and M. Mobarak, "Analysis of cutoff frequency in a one-dimensional superconductor-metamaterial photonic crystal," *Phys. C, Supercond. Appl.*, vol. 528, pp. 5–8, Sep. 2016.

[25] Y. Trabelsi, "Tunable properties of omnidirectional band gap based on photonic quasicrystals containing superconducting material," *Opt. Quantum Electron.*, vol. 53, no. 2, p. 76, Feb. 2021.

[26] O. Soltani, J. Zaghdoudi, and M. Kanzari, "Tunable filter properties in 1D linear graded magnetized cold plasma photonic crystals based on octonacci quasi-periodic structure," *Photon. Nanostruct.-Fundam. Appl.*, vol. 38, Feb. 2020, Art. no. 100744.

[27] K. V. Sreekanth *et al.*, "Extreme sensitivity biosensing platform based on hyperbolic metamaterials," *Nature Mater.*, vol. 15, no. 6, pp. 621–627, Jun. 2016.

[28] D. Rodrigo *et al.*, "Mid-infrared plasmonic biosensing with graphene," *Science*, vol. 349, no. 6244, pp. 165–168, 2015.

[29] M. Wuttig., H. Bhaskaran., and T. Taubner, "Phase-change materials for non-volatile photonic applications," *Nature Photon.*, vol. 11, pp. 465–476, Aug. 2017.

[30] P. Pitchappa, A. Kumar, S. Prakash, H. Jani, T. Venkatesan, and R. Singh, "Chalcogenide phase change material for active terahertz photonics," *Adv. Mater.*, vol. 31, no. 12, Mar. 2019, Art. no. 1808157.

[31] S. Abdollahramezani *et al.*, "Tunable nanophotonics enabled by chalcogenide phase-change materials," *Nanophotonics*, vol. 9, no. 5, pp. 1189–1241, 2020.

[32] C. Zhou *et al.*, "Optical radiation manipulation of Si-$Ge_2Sb_2Te_5$ hybrid metasurfaces," *Opt. Exp.*, vol. 28, no. 7, pp. 9690–9701, 2020.

[33] W. Zhu *et al.*, "Realization of a near-infrared active fano-resonant asymmetric metasurface by precisely controlling the phase transition of $Ge_2Sb_2Te_5$," *Nanoscale*, vol. 12, no. 16, pp. 8758–8767, 2020.

[34] S. Xiao *et al.*, "Active metamaterials and metadevices: A review," *J. Phys. D, Appl. Phys.*, vol. 53, no. 50, 2020, Art. no. 503002.

[35] J. Tian *et al.*, "Active control of anapole states by structuring the phase-change alloy $Ge_2Sb_2Te_5$," *Nature Commun.*, vol. 10, no. 1, p. 396, Dec. 2019.

[36] C. M. Chang, C. H. Chu, M. L. Tseng, H.-P. Chiang, M. Mansuripur, and D. P. Tsai, "Local electrical characterization of laser-recorded phase-change marks on amorphous $Ge_2Sb_2Te_5$ thin films," *Opt. Exp.*, vol. 19, no. 10, pp. 9492–9504, 2011.

[37] C. H. Chu *et al.*, "Laser-induced phase transitions of $Ge_2Sb_2Te_5$ thin films used in optical and electronic data storage and in thermal lithography," *Opt. Exp.*, vol. 18, no. 17, pp. 18383–18393, 2010.

[38] E. Zeidan, R. Shivaji, V. C. Henrich, and M. G. Sandros, "Nano-SPRi aptasensor for the detection of progesterone in buffer," *Sci. Rep.*, vol. 6, no. 1, pp. 1–8, Jul. 2016, doi: 10.1038/srep26714.

[39] A. Lieberman and L. Curtis, "In defense of progesterone: A review of the literature," *Alternative Therapies Health Med.*, vol. 23, no. 6, pp. 24–32, 2017.

[40] D. Tulchinsky and D. M. Okada, "Hormones in human pregnancy: IV. Plasma progesterone," *Amer. J. Obstetrics Gynecol.*, vol. 121, no. 3, pp. 293–299, 1975, doi: 10.1016/0002-9378(75)90001-0.

[41] D. Tulchinsky, C. J. Hobel, E. Yeager, and J. R. Marshall, "Plasma estrone, estradiol, estriol, progesterone, and 17-hydroxyprogesterone in human pregnancy: I. Normal pregnancy," *Amer. J. Obstetrics Gynecol.*, vol. 112, no. 8, pp. 1095–1100, 1972, doi: 10.1016/0002-9378(72)90185-8.

[42] D. L. Loriaux, H. J. Ruder, D. R. Knab, and M. B. Lipsett, "Estrone sulfate, estrone, estradiol and estriol plasma levels in human pregnancy," *J. Clin. Endocrinol. Metabolism*, vol. 35, no. 6, pp. 887–891, Dec. 1972, doi: 10.1210/jcem-35-6-887.

[43] M. Mihm, S. Gangooly, and S. Muttukrishna, "The normal menstrual cycle in women," *Animal Reproduction Sci.*, vol. 124, nos. 3–4, pp. 229–236, Apr. 2011, doi: 10.1016/j.anireprosci.2010.08.030.

[44] A. Panda, P. D. Pukhrambam, N. Ayyanar, and T. K. Nguyen, "Investigation of transmission properties in defective one dimensional superconductive photonic crystal for ultralow level bioethanol detection," *Optik*, vol. 245, Nov. 2021, Art. no. 167733.

[45] A. Panda, P. D. Pukhrambam, F. Wu, and W. Belhadj, "Graphene-based 1D defective photonic crystal biosensor for real-time detection of cancer cells," *Eur. Phys. J. Plus*, vol. 136, no. 8, p. 809, Aug. 2021.

[46] A. Panda and P. D. Pukhrambam, "A theoretical proposal of high performance blood components biosensor based on defective 1D photonic crystal employing WS_2, MoS_2 and graphene," *Opt. Quantum Electron.*, vol. 53, p. 357, Jun. 2021.

[47] A. Panda, P. D. Pukhrambam, and G. Keiser, "Realization of sucrose sensor using 1D photonic crystal structure vis-à-vis band gap analysis," *Microsyst. Technol.*, vol. 27, pp. 833–842, Aug. 2021.

[48] M. M. Abadla and A. H. Elsayed, "Detection and sensing of hemoglobin using one-dimensional binary photonic crystals comprising a defect layer," *Appl. Opt.*, vol. 59, no. 2, pp. 418–424, 2020.

[49] N. Ayyanar, K. V. Sreekanth, G. T. Raja, and M. S. M. Rajan, "Photonic crystal fiber-based reconfigurable biosensor using phase change material," *IEEE Trans. Nanobiosci.*, vol. 20, no. 3, pp. 338–344, Jul. 2021.

[50] Y. Wang *et al.*, "Highly-enhanced plasmonic biosensors based on atomically thin two-dimensional chalcogenide phase-change materials," in *Proc. Conf. Lasers Electro-Opt.*, 2020, pp. 1–2.

[51] S. K. Patel, J. Parmar, V. Sorathiya, T. K. Nguyen, and V. Dhasarathan, "Tunable infrared metamaterial-based biosensor for detection of hemoglobin and urine using phase change material," *Sci. Rep.*, vol. 11, no. 1, p. 7101, Dec. 2021.